

Modeling of Spiral-Wound Permeators for Multicomponent Gas Separations

Runhong Qi and Michael A. Henson*

Department of Chemical Engineering, Louisiana State University, Baton Rouge, Louisiana 70803-7303

Two multicomponent models for spiral-wound gas permeators are proposed. The basic transport model is derived from fundamental material balances and permeation relations that account for permeate-side pressure variations. The resulting model consists of a set of nonlinear differential–algebraic–integral equations with mixed boundary conditions, as well as an implicit expression for the local feed-side flow rate. The approximate model is derived from the basic model by assuming the residue flow rate is constant in the direction of bulk permeate flow. This assumption yields a set of nonlinear algebraic equations which can be solved very efficiently and reliably. The two models are compared for the separation of CO₂ from hydrocarbons in a four-component mixture, as well as the separation of an eight-component mixture. The models show close agreement for a wide range of operating conditions. An estimation technique for determining uncertain/unknown model parameters from experimental data also is proposed. The technique is successfully applied to data for a multicomponent mixture containing CO₂ and CH₄.

1. Introduction

In recent years, gas separation membranes have emerged as a viable alternative to more mature technologies such as absorption and cryogenic distillation. The use of spiral-wound permeators to separate gas mixtures encountered in natural gas treatment and enhanced oil recovery is one of the most important applications of membrane technology. However, the lack of appropriate permeator models is a major obstruction to effective simulation and design of membrane processes. Further improvements in spiral-wound membrane systems require the derivation of accurate permeator models which can be used to investigate separation performance and develop systematic design techniques.

A wide variety of permeator models has been reported for both binary and multicomponent gas mixtures (Kovvali *et al.*, 1992). The development of multicomponent transport models is of considerable practical significance since most industrial applications involve multicomponent separations. Multicomponent gas permeators with (Pan, 1986; Giglia *et al.*, 1991) and without (Brubaker and Kammermeyer, 1954; Pan and Habgood, 1978; Stern and Leone, 1980; Shindo *et al.*, 1985; Saltonstall, 1987; McCandless, 1990; Li *et al.*, 1990) permeate-side pressure drop have been investigated. For asymmetric membranes, Pan (1983) proposes that permeation occurs via a cross-flow pattern regardless of the flow direction of the bulk permeate stream. By using the local permeate composition rather than the bulk composition to characterize permeation, binary transport models for hollow-fiber and spiral-wound permeators with permeate-side pressure drop are derived (Pan, 1983). Pan (1986) also formulates a multicomponent hollow-fiber model that includes pressure drop inside the fiber. A multicomponent spiral-wound model without permeate-side pressure drop is proposed by Pan

and Habgood (1978). Surprisingly, we have not found multicomponent transport models of spiral-wound gas permeators which include permeate-side pressure variations.

Basic transport models with permeate-side pressure drop typically consist of nonlinear ordinary differential equations with mixed boundary conditions. These models can be solved with a trial-and-error shooting method that requires an initial guess of the permeate-side pressure distribution (Pan, 1983, 1986). The differential equations are solved to generate the outlet permeate concentration, as well as a new pressure distribution. The procedure is continued until the permeate concentration converges to the desired accuracy. This solution technique usually yields accurate results, but it is computationally expensive. As a result, basic transport models are difficult to use for process design.

An alternative approach is to develop approximate models which provide a more reasonable compromise between prediction accuracy and computational efficiency. Kovvali *et al.* (1994) propose an approximate modeling technique for multicomponent mixtures in which the hollow-fiber permeator is divided into small segments, and a linear relationship between the permeate-side and feed-side compositions in each segment is assumed. This assumption leads to a nonlinear algebraic equation model. However, the inherently nonlinear relationship between the permeate-side and feed-side compositions necessitates the use of a large number of segments (*e.g.*, 40), which significantly reduces the efficiency of the method. Chen *et al.* (1994) propose an average driving force approximation method for multicomponent separations. Under the assumption that the driving force for permeation is constant along the length of the hollow-fiber permeator, a nonlinear algebraic equation model is obtained by replacing the variable driving force with its arithmetic average. However, this assumption is valid only when variations in the feed-side and permeate-side concentrations are small. Pettersen and Lien (1994) developed an approximate modeling technique for multicomponent hollow-fiber permeators by assuming a logarithmic mean driving

* To whom correspondence should be addressed. Phone: 504-388-3690. Fax: 504-388-1476. E-mail: henson@nlc.che.lsu.edu.

force for permeation analogous to that used in heat exchanger modeling. Unfortunately, there is no obvious way to extend this method to spiral-wound permeators.

In a previous paper (Qi and Henson, 1996), we have developed an approximate modeling technique for spiral-wound permeators separating binary gas mixtures. The basic assumption employed is that the residue flow rate does not vary significantly in the direction of permeate flow. Under this assumption, the basic transport model proposed by Pan (1983) can be reduced to a small number of nonlinear algebraic equations. The approximate model provides very good agreement with the basic model, while requiring less than 1% of the computing effort.

In this paper, we present two multicomponent models for spiral-wound gas permeators. The *basic transport model* is derived directly from material balances and permeation relations assuming cross-flow patterns for bulk flow and local permeation. Permeate-side pressure variations are described by Darcy's law. As compared to the binary case, the principal difficulty is that the multicomponent model does not yield an explicit expression for the local feed-side flow rate. We show that the local feed-side flow rate and the local feed-side compositions can be calculated for a given permeate-side pressure distribution by solving an initial value problem. The basic transport equations then are solved via an iterative shooting method. The *approximate model* is derived directly from the basic transport model by assuming that the residue flow rate is constant along the direction of bulk permeate flow. Integral expressions are approximated via Gaussian quadrature, and the feed-side flow rate and compositions are determined by solving the associated initial value problem using a fourth-order Runge-Kutta-Gill algorithm. The basic and approximate models are compared for gas separations involving four and eight components. We show that the approximate model provides very close agreement while requiring significantly less computing effort. An estimation technique for determining uncertain/unknown model parameters from experimental data is proposed and applied to CO₂/CH₄ mixtures containing small amounts of N₂ and other hydrocarbons.

2. Basic Transport Model

Figure 1 shows the internal structure of a typical spiral-wound permeator (Coady and Davis, 1982; Mazur and Chan, 1982). The membrane element is constructed as follows. Spacing material is placed between two flat membrane sheets. Three edges of the two membrane sheets are sealed together, and the open edge is sealed to a perforated collection tube. A separator grid is placed on the top of the the resulting membrane leaf. The assembly is rolled around the collection tube and placed inside the cylindrical pressure vessel, resulting in a very large separation area per unit volume as compared to a simple plate-and-frame configuration.

The development of the basic transport model is based on Figure 2, which illustrates the feed and permeate flows in an extended membrane leaf. The variables are defined in the Nomenclature section. The feed stream is introduced on the outside of the leaf, and gas permeates through the two membranes into the spacing material. The more permeable components preferentially diffuse through the membranes in a cross-flow pattern, and the bulk permeate stream flows at a right angle with respect to the feed stream (*i.e.*, the *l*-direction shown in Figure 2). The feed-side gas that does not permeate is collected as the residue stream.

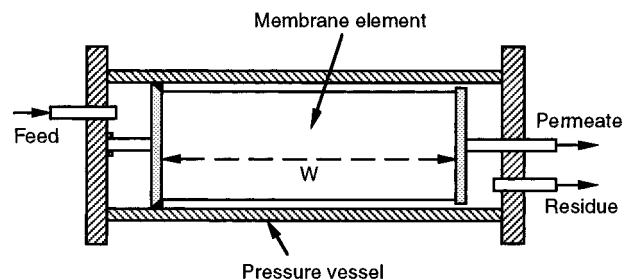


Figure 1. Spiral-wound membrane permeator.

The main assumptions employed are similar to those used in the binary case (Pan, 1983):

1. Permeation is described by a cross-flow pattern.
2. The feed-side pressure drop is negligible. This is a reasonable assumption for sufficiently low feed flow rates and/or short membrane leaf widths.
3. The porous supporting layer of the asymmetric membrane offers negligible resistance to gas flow.
4. There is no permeate mixing in the direction of bulk permeate flow.
5. The bulk permeate stream is accumulated by mixing the local permeate stream, which is perpendicular to the membrane surface, with the bulk permeate stream.
6. The permeate pressure varies only in the direction of permeate flow and the variations are described by Darcy's law (Bird *et al.*, 1960).
7. The membrane selectivities are independent of pressure and concentration.

2.1. Model Derivation. Under the preceding assumptions, the transport equations for a multicomponent spiral-wound permeator are as follows (Pan and Habgood, 1978; Pan, 1983):

permeation

$$\left[\frac{\partial(ux_i)}{\partial w} \right]_l = -2 \left(\frac{Q_i}{d} \right) (Px_i - py_i), \quad i = 1, \dots, n \quad (1)$$

$$\left[\frac{\partial(ux_i)}{\partial u} \right]_l = y'_i, \quad i = 1, \dots, n \quad (2)$$

permeate pressure

$$\frac{dp^2}{dl} = - \frac{2R_g T_l \mu V}{g_c W t B} \quad (3)$$

material balance

$$\frac{dV}{dl} = u_f - u_r \quad (4)$$

$$\frac{d(Vy_i)}{dl} = u_f x_{i,f} - u_r x_{i,r} \quad i = 2, \dots, n \quad (5)$$

composition sums

$$\sum_{i=1}^n x_i = 1, \quad \sum_{i=1}^n y_i = 1, \quad \sum_{i=1}^n y'_i = 1 \quad (6)$$

The variables are defined in the Nomenclature section. Although only $n - 1$ equations in (1) and (2) are independent, we list all the equations to facilitate the

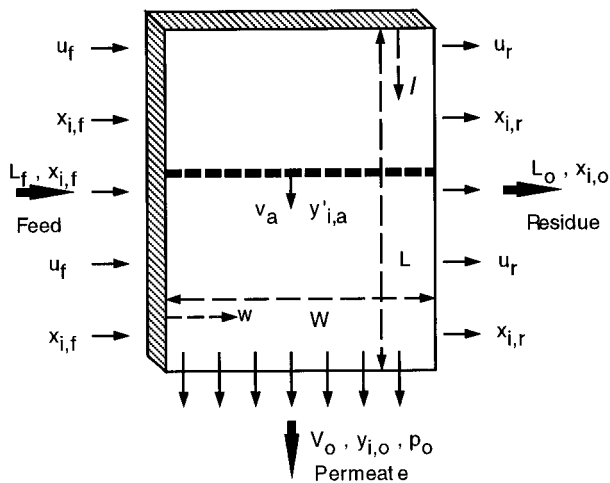


Figure 2. Gas permeation through an extended spiral-wound membrane.

subsequent development. Equations (1)–(5) can be rewritten in the following dimensionless form:

$$\left[\frac{\partial(Ux_p)}{\partial r} \right]_h = -\alpha_i(x_i - \gamma y_i), \quad i = 1, \dots, n \quad (7)$$

$$\left[\frac{\partial(Ux_p)}{\partial U} \right]_h = y'_i \quad i = 1, \dots, n \quad (8)$$

$$\frac{d\gamma^2}{dh} = -C\theta \quad (9)$$

$$\frac{d\theta}{dh} = 1 - U_r \quad (10)$$

$$\frac{d(\theta y_i)}{dh} = x_{i,f} - U_r x_{i,r} \quad i = 2, \dots, n \quad (11)$$

where

$$r = \left(\frac{2Q_b P}{du_f} \right) w \quad (12)$$

$$C = \frac{2R_g T_i L^2 u_f}{g_c W t B P^2} = \frac{2R_g T_i L L_f}{g_c W t B P^2} \quad (13)$$

The subscript *b* represents the base component to which the selectivities α_i are referred (*i.e.*, $\alpha_b = 1$). The base component can be any component for which $Q_b \neq 0$.

Equation (8) may be written as

$$\left[\frac{\partial(\ln U)}{\partial x_i} \right]_h = \frac{1}{y'_i - x_i}, \quad i = 1, \dots, n \quad (14)$$

Dividing (7) by (8) yields

$$\left[\frac{\partial U}{\partial r} \right]_h = -\frac{x_i - \gamma y'_i}{y'_i / \alpha_i}, \quad i = 1, \dots, n \quad (15)$$

Using (6), the right-hand side of (15) can be summed from $i = 1$ to n without changing the ratio value, which

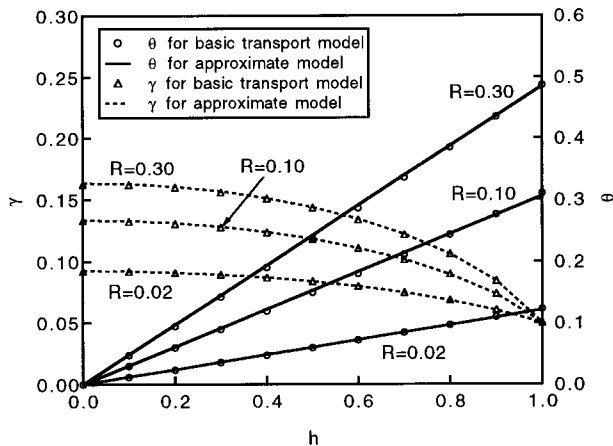
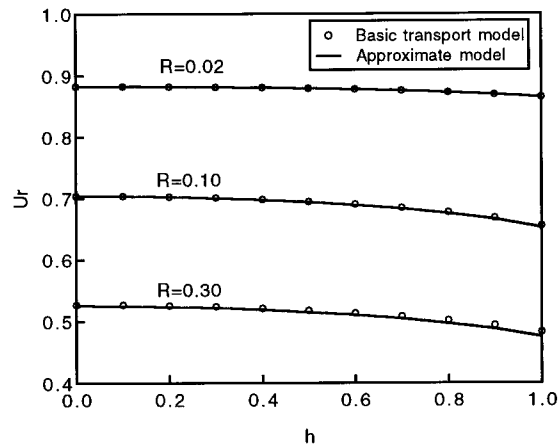


Figure 3. Variations of residue flow rate, permeate pressure, and permeate flow rate along the membrane length.

yields

$$\frac{x_i - \gamma y'_i}{y'_i / \alpha_i} = \frac{\sum_{i=1}^n (x_i - \gamma y'_i)}{\sum_{i=1}^n (y'_i / \alpha_i)} = \frac{1 - \gamma}{y'_m} \quad (16)$$

where

$$y'_m = \sum_{i=1}^n \frac{y'_i}{\alpha_i} \quad (17)$$

Therefore

$$\left[\frac{\partial U}{\partial r} \right]_h = -\frac{1 - \gamma}{y'_m} \quad (18)$$

The following relations between the feed-side and permeate-side compositions are obtained from (16):

$$x_i = \gamma y'_i + \frac{(1 - \gamma) y'_i}{\alpha_i y'_m} \quad (19)$$

$$y'_i = \frac{\alpha_i x_i y'_m}{1 - \gamma + \gamma \alpha_i y'_m} \quad (20)$$

$$\sum_{i=1}^n \frac{\alpha_i x_i y'_m}{1 - \gamma + \gamma \alpha_i y'_m} = 1 \quad (21)$$

Note that the dimensionless permeate pressure γ only

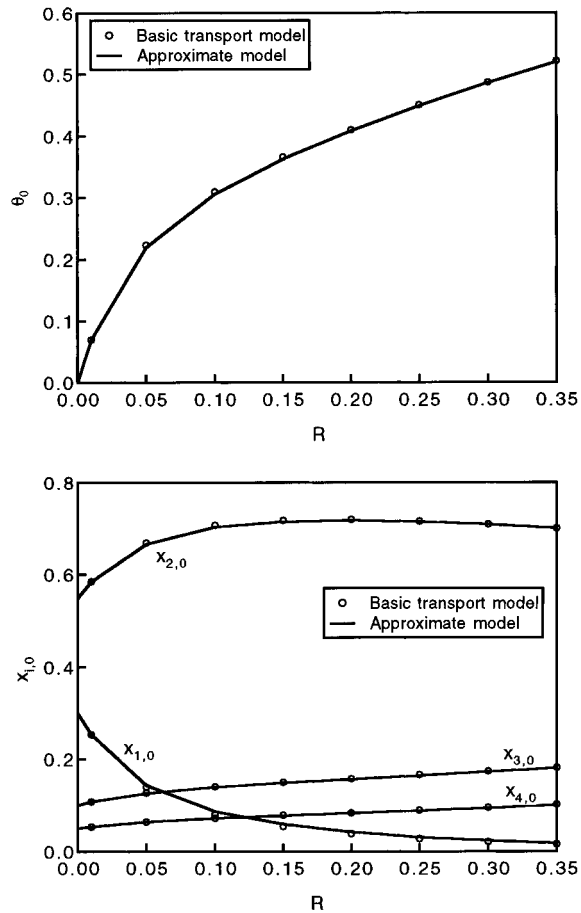


Figure 4. Effect of permeation factor on permeate flow rate and residue concentrations (four component system).

is a function of h from assumption 6; thus, (19)–(21) relate x_i , y'_i , and y'_m at a constant value of h . Therefore, substituting (19) into (14) yields the following relations at constant h (or γ):

$$d(\ln U) = \frac{1 + \gamma(\alpha_i y'_m - 1)}{(1 - \gamma)(\alpha_i y'_m - 1)} \frac{dy'_i}{y'_i} - \frac{dy'_m}{(\alpha_i y'_m - 1)y'_m}, \quad i = 1, \dots, n \quad (22)$$

Equations (19)–(22) are similar to expressions derived by Pan (1986) in modeling multicomponent hollow-fiber permeators. However, Pan's model contains differential equations with several independent variables. As a result, the model is difficult to solve. Below we reformulate the model equations to facilitate numerical solution by allowing y'_m to be the only independent variable.

Rearranging (22) to express dy'_i in terms of $d(\ln U)$ and dy'_m and then taking the sum from $i = 1$ to n , noting that $\sum_1^n dy'_i$ yields an expression for $d(\ln U)$ in terms of dy'_m :

$$\frac{d(\ln U)}{dy'_m} = - \frac{\sum_{j=1}^n A_j y'_j}{\sum_{j=1}^n B_j y'_j} \quad (23)$$

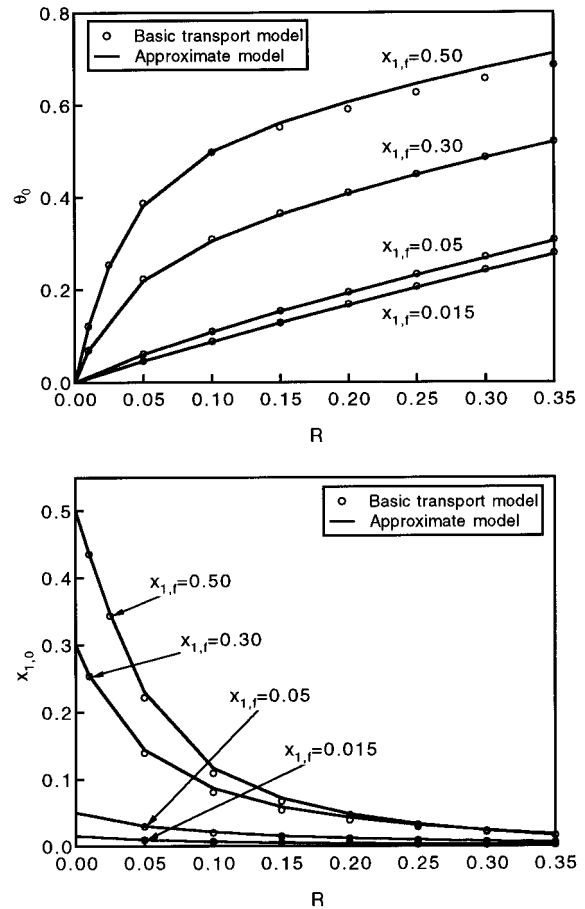


Figure 5. Effect of feed composition on permeate flow rate and residue concentration of the first component (four component system).

where:

$$A_j = \frac{1 - \gamma}{(1 - \gamma + \gamma \alpha_j y'_m) y'_m} \quad (24)$$

$$B_j = \frac{(1 - \gamma)(\alpha_j y'_m - 1)}{1 - \gamma + \gamma \alpha_j y'_m} \quad (25)$$

Substituting $d(\ln U)$ from (23) into (22) and choosing $n - 1$ independent equations yields dy'_i in terms of dy'_m :

$$\frac{dy'_i}{dy'_m} = y'_i \left(A_i - \frac{B_i \sum_{j=1}^n A_j y'_j}{\sum_{j=1}^n B_j y'_j} \right) \quad i = 2, \dots, n \quad (26)$$

At constant γ , solving (23) and (26) simultaneously and then using (6) to determine the composition of the first component yields functions $U(y'_m)$ and $y'_i(y'_m)$. Integrating (18) at constant γ with the boundary conditions

$$w = 0, \quad r = 0, \quad U = U_f = 1, \quad y'_m = y'_{m,f}$$

$$w = W, \quad r = R, \quad U = U_r, \quad y'_m = y'_{m,r}$$

yields

$$R = - \frac{1}{1 - \gamma} \int_1^{U_r} y'_m dU = \frac{1}{1 - \gamma} (y'_{m,f} - U_r y'_{m,r} + \int_{y'_{m,f}}^{y'_{m,r}} U dy'_m) \quad (27)$$

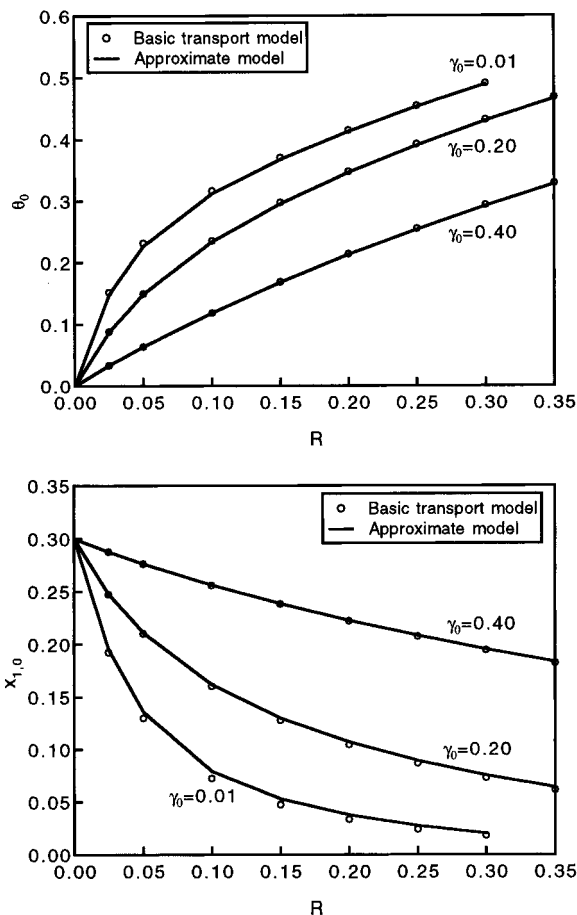


Figure 6. Effect of permeate pressure on permeate flow rate and residue concentration of the first component (four component system).

where R is the dimensionless permeation factor:

$$R = \frac{2Q_b WP}{du_f} = \frac{2Q_b LWP}{dL_f} \quad (28)$$

Equations (9)–(11), (19)–(21), (23), (26), and (27) represent the multicomponent transport model for the spiral-wound permeator.

2.2. Calculation Procedure. The multicomponent model can be solved via an iterative shooting method. As compared to the binary case discussed by Pan (1983), the major difficulty in solving the multicomponent model is that an explicit expression for the dimensionless residue flow rate U_r is not available. Consequently, for each step in integrating the differential equations (10) and (11), the initial-value differential equations (23) and (26) and the nonlinear algebraic equation (27) must be solved to obtain $U_r(h)$ and $x_{i,r}(h)$. As shown below, this makes the calculation procedure very complicated and time consuming.

For a spiral-wound permeator with specified separation properties (α_i , R , and C), outlet pressure ratio (γ_0), and feed composition ($x_{i,f}$), the iterative solution procedure may be outlined as follows:

1. Calculation of U_r and $x_{i,r}$ for a given value of γ .
 - (a) For a given $x_{i,f}$, solve (21) for $y'_{m,f}$ and use (20) to calculate $y'_{i,f}$.
 - (b) Solve (23), (26), and (27) simultaneously with initial conditions $y'_m = y'_{m,f}$, $y'_i = y'_{i,f}$, and $U = U_f = 1$ to obtain $y'_{m,r}$, $y'_{i,r}$, and U_r , and then calculate $x_{i,r}$ using (19).
2. Shooting method to solve the differential equations (9)–(11).

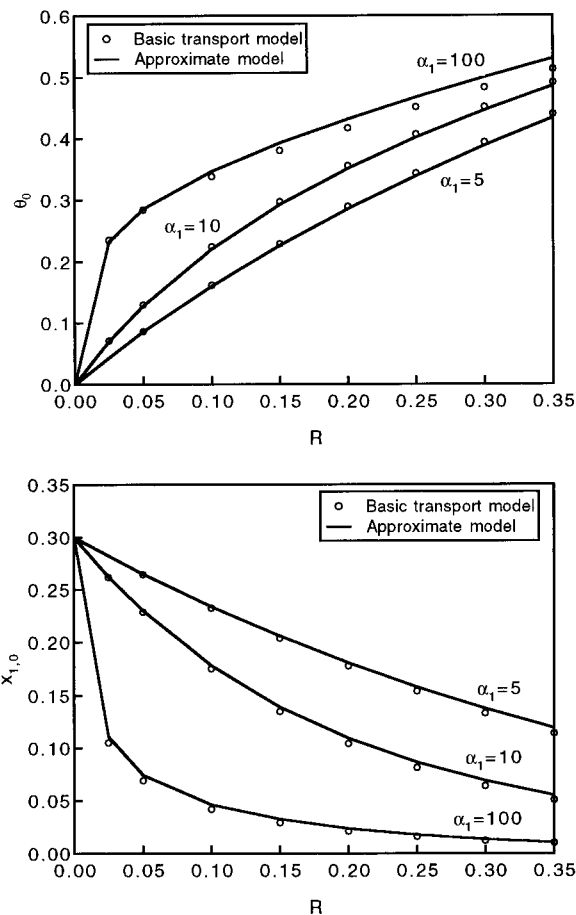


Figure 7. Effect of selectivity on permeate flow rate and residue concentration of the first component (four component system).

- (a) Initially assume that γ is equal to γ_0 for all h .
- (b) Using this $\gamma-h$ relation and the calculation procedure in step 1, integrate (10) and (11) from $h = 0$ (where $\theta = \theta_{y_i} = 0$) to $h = 1$ to obtain $\theta-h$ and y_i-h relations and then evaluate the relations at $h = 1$ to obtain θ_0 and $y_{i,0}$.
- (c) Utilizing the $\theta-h$ relation obtained in step 2b, integrate (9) from $h = 1$ (where $\gamma = \gamma_0$) to $h = 0$ to obtain a new $\gamma-h$ relation.
- (d) Repeat steps 2b and 2c until θ_0 converges to the desired accuracy. The outlet residue stream flow rate and concentrations are calculated by the overall material balance.

3. Approximate Model

3.1. Model Development. As in the binary case (Qi and Henson, 1996), the approximate model is developed by assuming that the residue flow rate U_r is constant with respect to h in order to develop an approximate pressure distribution function $\gamma(h)$. It is important to note that U_r is allowed to vary with h in the subsequent model development. Under this assumption, the differential equation (10) for the dimensionless permeate flow rate is easily integrated with boundary condition $\theta(0) = 0$:

$$\theta = (1 - U_r)h \quad (29)$$

In section 4 we show this assumption is valid for a wide range of operating conditions by demonstrating that U_r exhibits a very weak dependence on h , while θ effectively is a linear function of h . Substitution of (29) into (9) and integration with the boundary condition

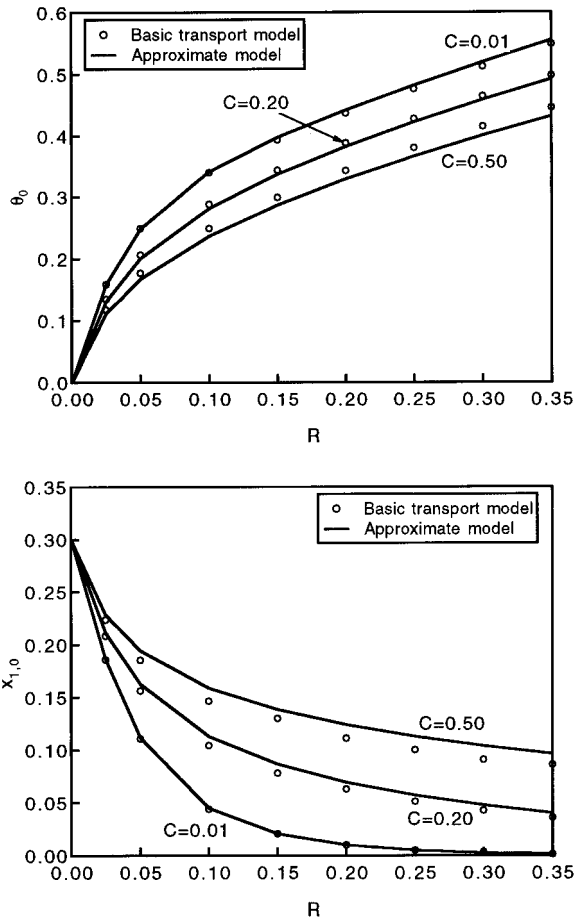


Figure 8. Effect of dimensionless constant C on permeate flow rate and residue concentration of the first component (four component system).

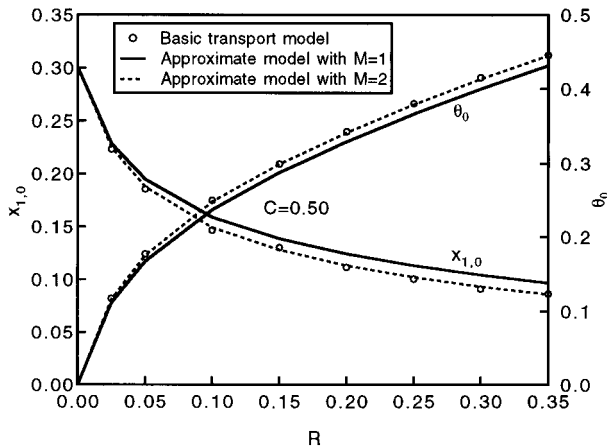


Figure 9. Accuracy improvement of the approximate model by increasing the number of quadrature points M .

$\gamma(1) = \gamma_0$ yields the approximate pressure distribution function:

$$\gamma^2 = \gamma_0^2 + \frac{1}{2}C(1 - U_p)(1 - h^2) \quad (30)$$

The subsequent model development is based on this $\gamma-h$ relation.

The integral in (27) is approximated using Gaussian quadrature (Rice and Do, 1995):

$$I \equiv \int_{y_{m,f}}^{y_{m,r}} U dy_m \approx (y_{m,r} - y_{m,f}) \sum_{j=1}^N U_j w_j \quad (31)$$

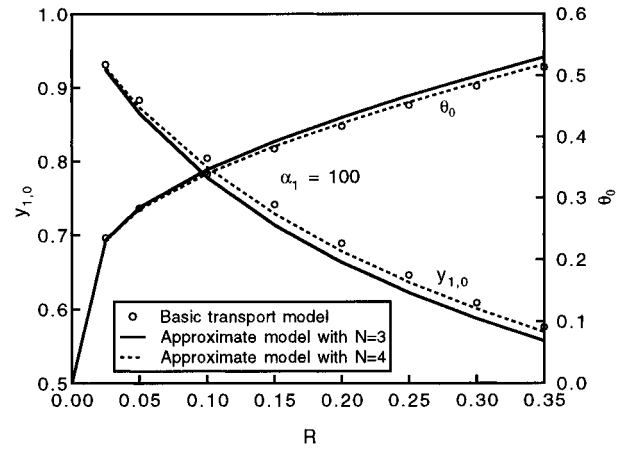


Figure 10. Accuracy improvement of the approximate model by increasing the number of quadrature points N .

where

$$y'_{m,j} = y'_{m,f} + \xi_j(y'_{m,r} - y'_{m,f}) \quad (32)$$

Here N is the number of quadrature points, ξ_j and w_j are the quadrature points and quadrature weights, respectively, and U_j is the feed-side flow rate at the quadrature point $y_{m,j}$. Now the integral equation (27) can be represented as

$$R = \frac{1}{1 - \gamma} (y'_{m,f} - U_r y'_{m,r} + (y'_{m,r} - y'_{m,f}) \sum_{j=1}^N U_j w_j) \quad (33)$$

The flow rates U_j and U_r are obtained by integrating the initial-value differential equations (23) and (26). Numerical solutions are obtained by using a fourth-order Runge-Kutta-Gill approximation at each quadrature point $y'_{m,j}$ and the outlet point $y'_{m,r}$. The resulting expressions are (Rice and Do, 1995)

$$Y_j = Y_{j-1} + \frac{1}{6}(K_1 + K_4) + \frac{1}{3}(\lambda_2 K_2 + \lambda_4 K_3) \quad (34)$$

$$K_1 = \delta_j F(y'_{m,j-1}, Y_{j-1}) \quad (35)$$

$$K_2 = \delta_j F\left(y'_{m,j-1} + \frac{\delta_j}{2}, Y_{j-1} + \frac{1}{2}K_1\right) \quad (36)$$

$$K_3 = \delta_j F\left(y'_{m,j-1} + \frac{\delta_j}{2}, Y_{j-1} + \lambda_1 K_1 + \lambda_2 K_2\right) \quad (37)$$

$$K_4 = \delta_j F(y'_{m,j-1} + \delta_j, Y_{j-1} + \lambda_3 K_2 + \lambda_4 K_3) \quad (38)$$

where

$$Y_j = [\ln U_j, y'_{2,j}, \dots, y'_{n,j}]^T \quad (39)$$

$$F = [f_1, f_2, \dots, f_n]^T \quad (40)$$

$$\delta_j = y'_{m,j} - y'_{m,j-1} \quad (41)$$

$$\lambda_1 = \frac{\sqrt{2}-1}{2}, \quad \lambda_2 = \frac{2-\sqrt{2}}{2}, \quad \lambda_3 = -\frac{\sqrt{2}}{2}, \quad \lambda_4 = \frac{2+\sqrt{2}}{2} \quad (42)$$

The functions f_1, f_2, \dots, f_n represent the right-hand sides of (23) and (26), and $y'_{i,j}$ represents the permeate

concentration of the i th component at the quadrature point $y_{m,j}$. The initial conditions are

$$Y_0 = [0, y'_{2,f}, \dots, y'_{n,f}]^T \quad (43)$$

where $y'_{i,f}$ is determined from $y'_{m,f}$ using (20). Equations (34)–(38) represent n nonlinear algebraic equations that must be solved simultaneously at each quadrature point and the outlet point to yield U_j , $y'_{i,j}$, U_r , and $y'_{i,r}$ for $i = 2, \dots, n$. Note that (34)–(38) are solved for a given value of γ , and therefore y'_m is the only independent variable. When γ is taken as a variable, the resulting functions for U_r and $y'_{i,r}$ can be expressed as

$$U_r = \Phi_1(\gamma, y'_{m,f}, y'_{m,r}) \quad (44)$$

$$y'_{i,r} = \Phi_i(\gamma, y'_{m,f}, y'_{m,r}), \quad i = 2, \dots, n \quad (45)$$

Substitution of U_j and U_r into (33) yields the relation

$$R = \Psi(\gamma, y'_{m,f}, y'_{m,r}) \quad (46)$$

Simultaneous solution of the nonlinear algebraic equations (21), (30), (44), and (46) at each quadrature point yields $y'_{i,f}(h_k)$, $\gamma(h_k)$, $U_r(h_k)$, and $y'_{m,r}(h_k)$, where h_k represents the value of h at the k th quadrature point. Substitution of these variables into (45) yields $y'_{i,r}(h_k)$, which then is used to calculate $x_{i,r}(h_k)$ via (19).

As in the binary case (Qi and Henson, 1996), Gaussian quadrature is used to determine the effluent permeate flow rate and bulk concentration. From (10):

$$\theta_0 = 1 - \int_0^1 U_r \cong 1 - \sum_{k=1}^M U_r(h_k) w_k \quad (47)$$

where M is the number of quadrature points employed, w_k are the quadrature weights, and $U_r(h_k)$ is the value of U_r at the k th quadrature point. By performing a material balance on a differential length of membrane and invoking the assumption that U_r does not vary with h , the permeate compositions are approximated as (Qi and Henson, 1996)

$$y_{i,0} = \int_0^1 y'_{i,a} dh \cong \sum_{k=1}^M y'_{i,a}(h_k) w_k, \quad i = 2, \dots, n \quad (48)$$

where

$$y'_{i,a}(h_k) = \frac{x_{i,f} - x_{i,r}(h_k)U_r(h_k)}{1 - U_r(h_k)}, \quad i = 2, \dots, n \quad (49)$$

The bulk concentration for the first component is determined via (6). The flow rate η_0 and bulk concentration $x_{i,0}$ of the effluent residue stream are determined from an overall material balance about the permeator:

$$\eta_0 = 1 - \theta_0 \quad (50)$$

$$x_{i,0} = \frac{x_{i,f} - \theta_0 y_{i,0}}{1 - \theta_0} \quad (51)$$

It will be shown that a single quadrature point ($M = 1$) provides a satisfactory solution for most operating conditions. In this case $h_1 = 0.5$ and $w_1 = 1$, and the quadrature formulas reduce to

$$\theta_0 = 1 - U_r(h_1) \quad (52)$$

$$y_{i,0} = y'_{i,a}(h_1) = \frac{x_{i,f} - x_{i,r}(h_1) U_r(h_1)}{1 - U_r(h_1)} \quad (53)$$

3.2. Parameter Estimation. A potential drawback of the proposed modeling approach is that detailed characteristics of spiral-wound permeators often are not known at the preliminary design stage. Consequently, the approximate model may contain uncertain and/or unknown parameters. One way to address this problem is to use estimation techniques to determine the model parameters from experimental data. For binary separation systems, we have developed a nonlinear programming strategy to estimate C (eq 13) and R (eq 28) by noting that all unknown parameters in the approximate model appear only via these two terms (Qi and Henson, 1996). Using the least-squares error between the measured variables and the estimated variables as the objective function and all binary model equations as constraints, "optimal" parameters are determined by solving a minimization problem. A similar technique could be developed for multicomponent systems by using the multicomponent model equations as constraints. Potential difficulties in using the multicomponent model for parameter estimation include the following: (1) the permeate concentrations for the least permeable components normally are very small; (2) the multicomponent model is considerably more complicated than the binary model. As a result, parameter estimation could be less reliable and less efficient than in the binary case.

A simplified method of parameter estimation for multicomponent systems may be developed by using the binary model. Similar to multicomponent distillation (King, 1980), we divide the different components into five groups according to their relative permeabilities. The most important two components are denoted as the light key component (LK) and heavy key component (HK). Components more permeable than the LK are called light components (L), while components less permeable than the HK are called heavy components (H). Components between the two key components are called intermediate components (I). A *sharp cut* is defined as a separation in which there are no heavy components in the permeate stream and no light components in the residue stream. By assuming a sharp cut, an analogous binary system may be constructed under the following conditions:

1. There are no light components or the concentrations of the light components are sufficiently small.

2. There are no intermediate components or the concentrations of the intermediate components are sufficiently small.

Under these conditions, we formulate a binary model by defining a relative flow rate, a relative pressure, and relative concentrations:

$$L_f^b = L_f(x_{f,LK} + x_{f,HK}) \quad (54)$$

$$P^b = P(x_{f,LK} + x_{f,HK}) \quad (55)$$

$$x_0^b = \frac{x_{f,LK}}{x_{f,LK} + x_{f,HK}} \quad (56)$$

$$\gamma_0^b = \frac{P_0}{P^b} = \frac{\gamma_0}{x_{f,LK} + x_{f,HK}} \quad (57)$$

$$\theta_0^b = \frac{V_0}{L_f^b} = \frac{\theta_0}{x_{f,LK} + x_{f,HK}} \quad (58)$$

$$y_0^b = \frac{y_{0,LK}}{y_{0,LK} + y_{0,HK}} \quad (59)$$

Because the parameters C and R depend on the feed flow rate (L_f) and the feed pressure (P), we define two parameters C and R that do not vary with the operating conditions:

$$C = \frac{2R_g T \mu L}{g_c W t B} \quad (60)$$

$$R = \frac{2Q_b L W}{d} \quad (61)$$

From (13) and (28):

$$C = C \frac{L_f}{P^2} \quad (62)$$

$$R = R \frac{P}{L_f} \quad (63)$$

In this way, the multicomponent estimation problem is reduced to estimating the parameters C and R using the binary model and the binary variables. Detailed formulation of the estimation problem is described in a previous paper (Qi and Henson, 1996).

4. Case Studies

We compare the basic transport model and the approximate model for the separation of gas mixtures containing four and eight components. The four-component example involves CO₂ separation from a hydrocarbon mixture containing CH₄, C₂H₆, and C₃H₈ (Pan, 1986). The eight-component example does not represent any specific gas separation system, but it does demonstrate the potential for modeling mixtures with a large number of components. The proposed models are evaluated for a wide range of model parameters and operating conditions. In addition, the parameter estimation technique is applied to experimental data for the separation of CO₂/CH₄ mixtures containing small amounts of N₂ and other hydrocarbons (Lee and Feldkirchner, 1993).

For binary mixtures, the multicomponent models yield the same results as binary models (Qi and Henson, 1996). The models differ only because an explicit expression for the feed-side flow rate cannot be derived in the multicomponent case. In this sense, the multicomponent models can be regarded as generalizations of the binary models. Therefore, results for binary mixtures are not shown here.

4.1. Four-Component System. The basic transport model and the approximate model are compared in Figures 3–10. Table 1 contains the parameter values not shown explicitly in each figure. The operating conditions are based on data from Pan (1986) for CO₂ separation from hydrocarbon mixtures containing CH₄, C₂H₆, and C₃H₈. The values of C and R are obtained from our previous study of binary separations (Qi and Henson, 1996). The approximate model is solved using three quadrature points for the integral (31) and one quadrature point for integrals (47) and (48) (*i.e.*, $N = 3$, $M = 1$). The second component CH₄ is chosen as the

Table 1. Nominal Operating Conditions for a Four-Component System^a

parameter	value	variable	BTM value	APM value
$x_{i,f}$	0.30	$x_{i,0}$	0.0808	0.0862
	0.55		0.7067	0.7027
	0.10		0.1405	0.1395
	0.05		0.0720	0.0715
α_i	30	$y_{i,0}$	0.7880	0.7845
	1		0.2011	0.2038
	0.25		0.0099	0.0104
	0.05		0.0010	0.0013
γ_0	0.05	η_0	0.6900	0.6939
C	0.1	θ_0	0.3100	0.3061
R	0.1			

^a BTM = basic transport model. APM = approximate model.

base component for calculating the selectivities α_i . Note that any component can be chosen as the base component, but the value of the permeation factor R is determined by the permeability of the selected component.

Figure 3 shows the residue flow rate U_r , permeate flow rate θ , and permeate-side pressure γ as a function of the membrane length h for three values of the permeation factor R . As assumed in the development of the approximate model, U_r is a weak function of h and θ exhibits a linear dependence on h . The approximate model produces very accurate predictions of the three variables for each value of R . Figure 4 illustrates the effect of R on the outlet permeate flow rate θ_0 and the outlet residue concentration $x_{i,0}$ for all four components. The two models yield almost identical predictions for all values of R . Note that, as R increases, the residue concentration of the most permeable component ($x_{1,0}$) decreases, the concentration of the moderately permeable component ($x_{2,0}$) exhibits a maximum, and the concentrations of the least permeable components ($x_{3,0}$ and $x_{4,0}$) increase.

The permeate flow rate θ_0 and the residue concentration of the first component $x_{1,0}$ for various combinations of R and the feed concentrations $x_{i,f}$ are shown in Figure 5. The concentrations of components 1 and 2 are changed to keep the sum of the mole fraction unity, while the concentrations of components 3 and 4 are the same as shown in Table 1. The predictions of θ_0 and $x_{1,0}$ obtained from the approximate model are very accurate except for small deviations at large values of $x_{1,f}$ and R . Figure 6 shows the effect of R and the outlet permeate pressure γ_0 on θ_0 and $x_{1,0}$. The two models show very close agreement for all operating conditions considered. The effect of R and the selectivity on θ_0 and $x_{1,0}$ is illustrated in Figure 7. The selectivity of the first component α_1 is changed, while the selectivities of the other components remain constant. The predictions of the approximate model are very accurate for most conditions, although small deviations in θ_0 are observed for large values of R and α_1 . Figure 8 shows the effect of R and the parameter C on θ_0 and $x_{1,0}$. The approximate model produces accurate predictions for low values of C , but deviations are observed as C is increased. This is expected as the approximate pressure distribution function (30) becomes less accurate as C increases.

The results in Figures 7 and 8 show that the approximate model becomes less accurate for large values of α_1 and C . The accuracy of the approximate model can be improved by increasing the numbers of quadrature points used to approximate integrals in the basic transport model. Figure 9 shows the improvement obtained when the number of quadrature points in (47) is changed from $M = 1$ to $M = 2$. The operating

Table 2. Nominal Operating Conditions for an Eight-Component System^a

parameter	value	variable	BTM value	APM value
$x_{i,f}$	0.20	$x_{i,0}$	0.0664	0.0697
	0.20		0.1259	0.1281
	0.20		0.1973	0.1974
	0.20		0.2750	0.2729
	0.05		0.0778	0.0771
	0.05		0.0830	0.0822
	0.05		0.0864	0.0855
	0.05		0.0882	0.0872
α_i	20	$y_{i,0}$	0.3724	0.3723
	10		0.2957	0.2951
	5		0.2035	0.2035
	2		0.1032	0.1036
	1		0.0141	0.0142
	0.5		0.0074	0.0074
	0.2		0.0030	0.0031
	0.05		0.0008	0.0008
γ_0	0.05	η_0	0.5634	0.5694
C	0.1	θ_0	0.4366	0.4306
R	0.1			

^a BTM = basic transport model. APM = approximate model.

conditions are identical to those in Figure 8 for $C = 0.50$. The approximate model produces very accurate results when $M = 2$. Figure 10 shows the improvement obtained by increasing the number of quadrature points in (31) from $N = 3$ to $N = 4$. The operating conditions are the same as in Figure 7 for $\alpha_1 = 100$. In this case, we show predictions of the permeate concentration $y_{1,0}$ rather than $x_{1,0}$ because the differences are more pronounced. As expected, improved accuracy is obtained when $N = 4$. Accuracy of the approximate model also can be improved by adding some intermediate points between the N quadrature points when performing integration via the Runge–Kutta–Gill algorithm (34)–(38); this does not require N to be increased. Note that the computation time increases almost linearly with the increase in M , while increasing N has much less effect.

The results in Figures 3–10 demonstrate that the approximate model provides very close agreement to the basic transport model for the four-component system over a wide range of operating conditions. The major advantage of the approximate model is that the resulting nonlinear algebraic equations can be solved very efficiently with little effect on prediction accuracy. On the other hand, solution of the basic transport model is very computationally intensive as a result of the nonlinear differential–algebraic–integral equations, mixed boundary conditions, and implicit expression for the feed-side flow rate. Running MATLAB on an IBM RS-6000 workstation, the computing time for a single simulation is 1.2–3 s with the approximate model as compared to 6–20 min with the basic model. Thus, the approximate model can be solved 200–600 faster than the basic transport model for the cases in Figures 3–10. This represents a substantial reduction in computing effort for the optimal design of complex permeator configurations, in which hundreds of model solutions may be required.

4.2. Eight-Component System. Figures 11–13 compare the basic transport model and the approximate model for an eight-component system. Operating conditions not shown explicitly in each figure are listed in Table 2. The fifth component is taken as the base component for determining α_i and R . As in the four-component case, Gaussian quadrature is performed with $M = 1$ and $N = 3$.

Figure 11 shows the outlet permeate flow rate θ_0 and the residue concentrations $x_{i,0}$ of all eight components

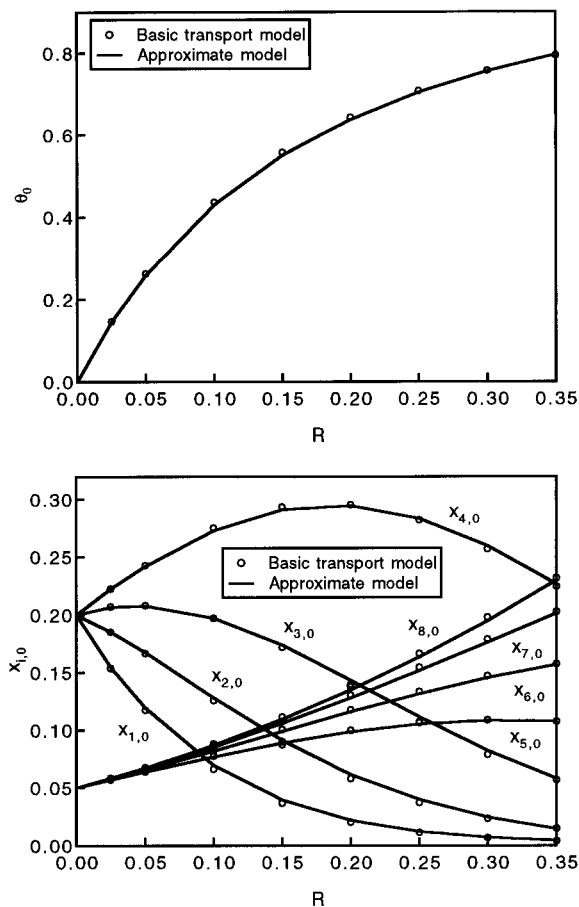


Figure 11. Effect of permeation factor on permeate flow rate and residue concentrations (eight-component system).

as a function of the permeation factor R . The two models produce almost identical results for all values of R . The effect of R and γ_0 on θ_0 and $x_{1,0}$ is shown in Figure 12. The approximate model yields accurate predictions for all operating conditions considered. Figure 13 shows the effect of R and C on θ_0 and $x_{1,0}$. The approximate model yields accurate predictions under most conditions, although small deviations are observed for large values of C as expected.

These results demonstrate that the basic transport model and the approximate model can be applied to gas mixtures with a large number of components. It is important to note that the computational effort associated with solving the approximate model does not increase dramatically as the number of components increases. The computing time for a single simulation in Figures 11–13 is 1.5–3.5 s with the approximate model and 8–25 min with the basic model. As in the four-component case, the approximate model is 200–700 times faster than the basic transport model.

4.3. Parameter Estimation. The effectiveness of the proposed parameter estimation strategy is investigated using experimental data for separation of CO_2/CH_4 mixtures containing small amounts of N_2 and other hydrocarbons (Lee and Feldkirchner, 1993). Nine sets of experimental data are selected for a permeator after checking the consistency of the operating temperature and the closure of material balances. The selectivities are chosen as in Lee *et al.* (1995): CO_2/CH_4 selectivity = 20; N_2/CH_4 selectivity = 1.0; $\text{C}^+\text{H}/\text{CH}_4$ selectivity = 0.4. The C^+H represents all the hydrocarbons higher than CH_4 , but it consists mostly of C_2H_6 . Parameter estimation is achieved by transforming the experimental measurements into relative values according to (54)–

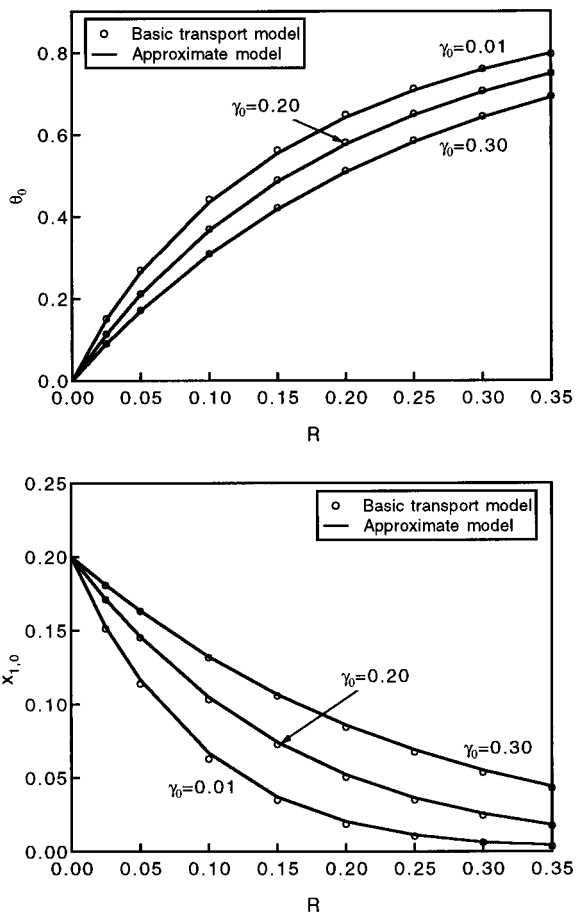


Figure 12. Effect of permeate pressure on permeate flow rate and residue concentration of the first component (eight-component system).

(59) and then using the binary model to estimate the parameters C and R (Qi and Henson, 1996). The estimation results are $C = 1.884 \times 10^{13} \text{ m}^3/\text{Pa}$ and $R = 3.578 \times 10^{-9} \text{ Pa}^2 \text{ s}/\text{m}^3$.

These parameters are used to simulate the multicomponent system. Table 3 shows the operating conditions and calculated C and R derived from the estimated C and R . Table 4 compares the experimental data and the predicted values, as well as their average relative errors. The θ_i and $y_{i,0}$ represent experimental measurements, and the $\hat{\theta}_i$ and $\hat{y}_{i,0}$ represent values predicted by the approximate multicomponent model using the estimated parameters. The errors are calculated as follows:

$$e_{\theta_0} = \frac{1}{N} \sum_{j=1}^N \left| \frac{\hat{\theta}_{0,j} - \theta_{0,j}}{\theta_{0,j}} \right| \times 100\% \quad (64)$$

$$e_{y,\rho} = \frac{1}{N} \sum_{j=1}^N \left| \frac{\hat{y}_{0,j} - y_{0,j}}{y_{0,j}} \right| \times 100\% \quad (65)$$

where N represents the number of experiments. The predictions are sufficiently accurate for preliminary process design. The large relative errors associated with the N_2 and C^+H components are attributable to their low concentrations in the permeate stream.

5. Summary and Conclusions

Two multicomponent models for spiral-wound gas permeators which include permeate-side pressure drop

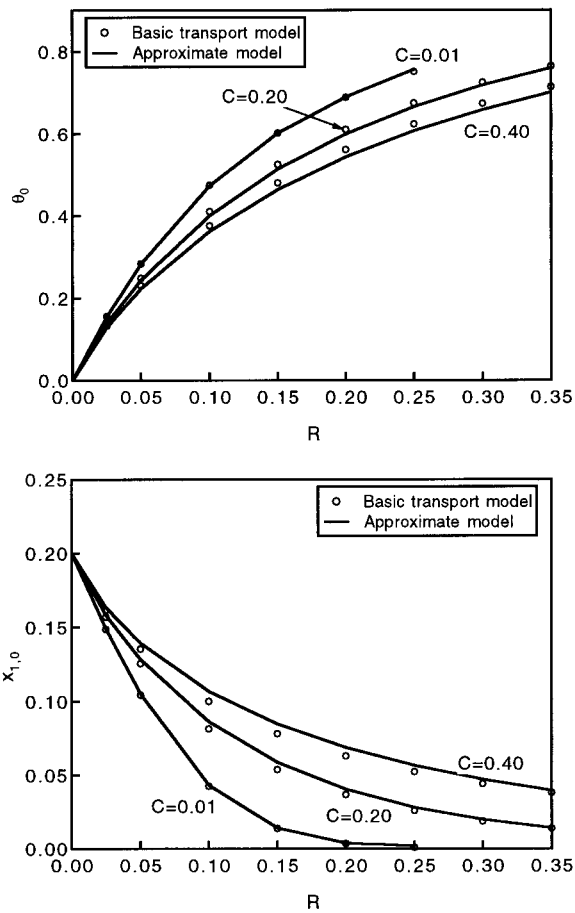


Figure 13. Effect of dimensionless constant C on permeate flow rate and residue concentration of the first component (eight-component system).

have been proposed. The basic transport model is derived from fundamental material balances and permeation relations, while the approximate model is derived directly from the basic model by assuming the residue flow rate is constant along the direction of permeate flow. The approximate model is developed by using Gaussian quadrature to approximate integral expressions and the fourth-order Runge–Kutta–Gill algorithm to solve the initial value problem for the feed-side flow rate and compositions. The two models compare favorably for gas mixtures containing four and eight components. The major shortcoming of the basic transport model is the computational effort required to generate a solution. On the other hand, the approximate model provides very accurate predictions with less than 1% of the computation time required for the basic model. In addition, a simple method for estimating uncertain/unknown model parameters from experimental data has been proposed and successfully applied to a CO_2/CH_4 separation system. As a result of its accuracy and efficiency, the approximate model is well suited for simulation and design of complex membrane separation systems.

Acknowledgment

Financial support from the Louisiana Quality Educational Support Fund (LEQSF(1993-96)-RD-B-03) is gratefully acknowledged.

Nomenclature

A_i = dimensionless constant defined by eq 24

Table 3. Operating Conditions and Parameters for Experimental Data (Lee and Feldkirchner, 1993)

no.	L_f (m ³ /s)	P (MPa)	γ_0	feed composition ($x_{i,f}$)				parameter	
				CO ₂	CH ₄	N ₂	C+H	R	C
1	0.0331	3.7557	0.0272	0.0523	0.8667	0.0122	0.0688	0.4058	0.0442
2	0.0318	2.3767	0.0429	0.0528	0.8686	0.0135	0.0651	0.2674	0.1061
3	0.0331	3.8247	0.0267	0.1161	0.8072	0.0114	0.0653	0.4133	0.0426
4	0.0466	3.2041	0.0318	0.1213	0.7969	0.0107	0.0711	0.2462	0.0854
5	0.0695	4.8589	0.0210	0.1234	0.8016	0.0105	0.0645	0.2501	0.0555
6	0.0692	3.9626	0.0258	0.1241	0.7959	0.0105	0.0695	0.2049	0.0830
7	0.0370	3.2386	0.0315	0.1272	0.7879	0.0105	0.0744	0.3128	0.0665
8	0.0774	4.8589	0.0210	0.1298	0.7905	0.0105	0.0692	0.2247	0.0617
9	0.0672	3.8936	0.0262	0.1339	0.7919	0.0105	0.0637	0.2073	0.0835

Table 4. Comparison of Experimental Data and Simulation Results

no.	cut ratio		outlet permeate composition ($y_{i,0}$)							
	θ_0	$\hat{\theta}_0$	CO ₂		CH ₄		N ₂		C+H	
			$y_{1,0}$	$\hat{y}_{1,0}$	$y_{2,0}$	$\hat{y}_{2,0}$	$y_{3,0}$	$\hat{y}_{3,0}$	$y_{4,0}$	$\hat{y}_{4,0}$
1	0.3762	0.4005	0.1318	0.1275	0.8214	0.8292	0.0095	0.0117	0.0373	0.0316
2	0.2887	0.2693	0.1564	0.1677	0.7911	0.7926	0.0089	0.0123	0.0436	0.0274
3	0.4059	0.4651	0.2676	0.2460	0.6908	0.7158	0.0077	0.0101	0.0339	0.0281
4	0.3310	0.3114	0.3345	0.3470	0.6275	0.6195	0.0064	0.0083	0.0316	0.0251
5	0.3538	0.3266	0.3319	0.3504	0.6308	0.6190	0.0062	0.0081	0.0311	0.0225
6	0.2796	0.2773	0.3732	0.3854	0.5956	0.5842	0.0059	0.0077	0.0253	0.0227
7	0.3628	0.3790	0.3212	0.3175	0.6398	0.6455	0.0069	0.0086	0.0321	0.0285
8	0.3051	0.3063	0.3766	0.3835	0.5928	0.5858	0.0066	0.0078	0.0240	0.0230
9	0.2537	0.2883	0.4081	0.4026	0.5590	0.5694	0.0056	0.0076	0.0273	0.0204
error (%)	6.740		3.942		1.528		29.04		18.73	

B = permeability of the spacing materials inside the spiral-wound leaf (m^2)

B_i = dimensionless constant defined by eq 25

C = dimensionless constant defined by eq 13

d = effective thickness of the membrane (m)

g_c = Newton's law conversion factor

h = l/L , dimensionless leaf length variable

h_k = quadrature points of h

l = membrane leaf length variable (m)

L = membrane leaf length (m)

L_f = feed gas flow rate per membrane leaf (mol/s)

L_o = residue gas flow rate per membrane leaf (mol/s)

M = number of quadrature points of θ_0 and $y_{i,0}$

N = number of quadrature points of the integral $I(\gamma, \gamma_{i,r})$

N = number of independent experiments in parameter estimation

P = feed-side pressure (Pa)

p = permeate-side pressure (Pa)

p_0 = permeate outlet pressure (Pa)

Q_i = permeabilities of the i th permeable component (mol·m·s⁻¹·Pa)

Q_b = permeability of the base component (mol/m·s·Pa)

r = dimensionless permeation variable defined by eq 12

R = dimensionless permeation factor defined by eq 28

R_g = ideal gas constant (m³·Pa/kg·mol·K)

s = w/W , dimensionless leaf width variable

t = membrane leaf thickness (m)

T = temperature (K)

U = u/u_f , dimensionless feed-side gas flow rate

U_j = dimensionless feed-side gas flow rate at j th quadrature point

U_r = u_r/u_f , dimensionless residue gas flow rate

u = feed-side gas flow rate per unit length of membrane leaf (mol/s·m)

u_f = feed gas flow rate per unit length of membrane leaf (mol/s·m)

u_r = residue gas flow rate per unit length of membrane leaf (mol/s·m)

V = permeate flow rate (mol/s)

V_0 = permeate flow rate at permeate outlet (mol/s)

v_a = permeate flow rate per unit length averaged over the width of the membrane (mol/s·m)

W = membrane leaf width (m)

w = membrane leaf width variable (m)

w_j = quadrature weight

x_j = local feed-side concentration (mole fraction)

$x_{i,0}$ = bulk residue stream concentration at outlet (mole fraction)

$x_{i,f}$ = feed concentration (mole fraction)

$x_{i,r}$ = local residue concentration along the outlet end of the membrane leaf (mole fraction)

y_i = permeate concentration in the bulk permeate stream (mole fraction)

$y_{i,0}$ = permeate concentration in the bulk permeate stream at the permeate outlet (mole fraction)

y'_i = local permeate concentration on the membrane surface (mole fraction)

$y'_{i,a}$ = local permeate concentration averaged over the width of the membrane (mole fraction)

$y'_{i,f}$ = local permeate concentration along the inlet end of the membrane leaf (mole fraction)

$y'_{i,j}$ = local permeate concentration at the j th quadrature point (mole fraction)

$y'_{i,r}$ = local permeate concentration along the outlet end of the membrane leaf (mole fraction)

y'_m = composition variable defined by eq 17

$y'_{m,f}$ = y'_m value at the feed inlet

$y'_{m,r}$ = y'_m value at the residue outlet

$y'_{m,j}$ = y'_m value at j th quadrature point

α_i = Q_i/Q_b , membrane selectivity for i th component

γ = p/P , ratio of permeate pressure to feed pressure

γ_0 = p_0/P , ratio of permeate pressure to feed pressure at the permeate outlet

μ = viscosity of gas mixture (Pa·s)

θ = V/L_f , ratio of permeate flow rate to feed flow rate

θ_0 = V_0/L_f , ratio of permeate flow rate to feed flow rate at permeate outlet

ξ_j = standard quadrature point

Φ_i = function expressed by eqs 44 and 45

Ψ = function expressed by eq 46

η_0 = L_0/L_f , ratio of residue outlet stream flow rate to feed flow rate

Literature Cited

- Bird, R. B.; Stewart, W. E.; Lightfoot, E. D. *Transport Phenomena*; Wiley International Edition: New York, 1960.
- Brubaker, D. W.; Kammermeyer, K. Separation of Gases by Plastic Membranes: Permeation Rates and Extent of Separation. *Ind. Eng. Chem.* **1954**, *46*, 733.

- Chen, H.; Jiang, G.; Xu, R. An Approximate Solution for Countercurrent Gas Permeation Separating Multicomponent Mixtures. *J. Membr. Sci.* **1994**, *95*, 11–19.
- Coady, A. B.; Davis, J. A. CO₂ Recovery by Gas Permeation. *Chem. Eng. Prog.* **1982**, 44–49.
- Giglia, S.; Bikson, B.; Perrin, J. E.; Donatelli, A. A. Mathematical and Experimental Analysis of Gas Separation by Hollow Fiber Membranes. *Ind. Eng. Chem. Res.* **1991**, *30*, 1239–1248.
- King, C. J. *Separation Processes*; McGraw-Hill: New York, 1980.
- Kovvali, A. S.; Vemury, S.; Krovvidi, K. R.; Khan, A. A. Models and Analyses of Membrane Gas Permeators. *J. Membr. Sci.* **1992**, *73*, 1–23.
- Kovvali, A. S.; Vemury, S.; Admassu, W. Modeling of Multicomponent Countercurrent Gas Permeators. *Ind. Eng. Chem. Res.* **1994**, *33*, 896–903.
- Lee, A. L.; Feldkirchner, H. L. Development of a Database for Advanced Processes to Remove Carbon Dioxide from Subquality Natural Gas. Topical Report GRI-93/0247. Gas Research Institute: Chicago, IL, 1993.
- Lee, A. L.; Feldkirchner, H. L.; Stern, S. A.; Houde, A. Y.; Gamez, J. P.; Meyer, H. S. Field Tests of Membrane Modules for the Separation of Carbon Dioxide for Low-Quality Natural Gas. *Gas Sep. Purif.* **1995**, *9*, 35–43.
- Li, K.; Acharya, D. R.; Hughes, R. Mathematical Modelling of Multicomponent Membrane Permeators. *J. Membr. Sci.* **1990**, *52*, 205–219.
- Mazur, W. H.; Chan, M. C. Membranes for Natural Gas Sweetening and CO₂ Enrichment. *Chem. Eng. Prog.* **1982**, 38–43.
- McCandless, F. P. Iterative Solution of Multicomponent Permeator Model Equations. *J. Membr. Sci.* **1990**, *48*, 115.
- Pan, C. Y. Gas Separation by Permeators with High-Flux Asymmetric Membranes. *AIChE J.* **1983**, *29*, 545–552.
- Pan, C. Y. Gas Separation by High-Flux, Asymmetric Hollow-Fiber Membrane. *AIChE J.* **1986**, *32*, 2020–2027.
- Pan, C. Y.; Habgood, H. W. Gas Separation by Permeation: Part I. Calculation Methods and Parametric Analysis. *Can. J. Chem. Eng.* **1978**, *56*, 197–209.
- Pettersen, T.; Lien, K. M. A New Robust Design Model for Gas Separating Membrane Modules Based on Analogy with Countercurrent Heat Exchangers. *Comput. Chem. Eng.* **1994**, *18*, 427–439.
- Qi, R.; Henson, M. A. Approximate Modeling of Spiral-Wound Gas Permeators. *J. Membr. Sci.* **1996**, *121*, 11–24.
- Rice, R. G.; Do, D. D. *Applied Mathematics and Modeling for Chemical Engineers*; Wiley: New York, 1995.
- Saltonstall, C. W. Calculation of Membrane Area Required for Gas Separations. *J. Membr. Sci.* **1987**, *32*, 185.
- Shindo, Y.; Hakuta, T.; Yoshitome, H.; Inoue, H. Calculation Methods for Multicomponent Gas Separation by Permeation. *Sep. Sci. Technol.* **1985**, *20*, 445–459.
- Stern, S. A.; Leone, S. M. Separation of Krypton and Xenon by Selective Permeation. *AIChE J.* **1980**, *26*, 881.

Received for review November 4, 1996

Revised manuscript received January 27, 1997

Accepted February 19, 1997[®]

IE960701Y

[®] Abstract published in *Advance ACS Abstracts*, April 15, 1997.